A contact area function for Berkovich nanoindentation: Application to hardness determination of a TiHfCN thin film

D. Chicot [a,*], M. Yetna N'Jock [a], E.S. Puchi-Cabrera [a,b,c], A. Iost [d], M.H. Staia [b], G. Louis [e], G. Bouscarrat [f], R. Aumaitre [f]

[a] Université Lille Nord de France, USTL, LML, CNRS, UMR 8107, F-59650 Villeneuve d'Ascq, France
[b] School of Metallurgical Engineering and Materials Science, Faculty of Engineering, Universidad Central de Venezuela, 47885, Los Chaguaramos, Caracas 1041, Venezuela
[c] Venezuelan National Academy for Engineering and Habitat, Palacio de las Academias, 1723, Caracas 1010, Venezuela
[d] MSMP, Arts et Métiers ParisTech, 8, Boulevard Louis XIV, 59000 Lille Cedex, France
[e] Mines Douai, LGCgE, F-59500 Douai, France
[f] Centre d'Ingénierie en Traitements et Revêtements de surface Avancées, CITRA, ENSIL, F-87068 Limoges, France

Keywords:
Nanoindentation
Contact area
Elastic modulus
Hardness
Thin film

A B S T R A C T

In nanoindentation, especially at very low indenter displacements, the indenter/material contact area must be defined in the best possible way in order to accurately determine the mechanical properties of the material. One of the best methodologies for the computation of the contact area has been proposed by Oliver and Pharr [W.C. Oliver, G.M. Pharr, J. Mater. Res. 7 (1992) 1564], which involves a complex phenomenological area function. Unfortunately, this formulation is only valid when the continuous stiffness measurement mode is employed. For other conditions of indentation, different contact area functions, which take into account the effective truncation length or the radius of the rounded indenter tip, as well as some fitting parameters, have been proposed. However, most of these functions require a calibration procedure due to the presence of such parameters. To avoid such a calibration, in the present communication a contact area function only related to the truncation length representative of the indenter tip defect, which can be previously estimated with high resolution microscopy, has been proposed. This model allows the determination of consistent indentation data from indenter displacements of only few nanometers in depth. When this proposed contact area function is applied to the mechanical characterization of a TiHfCN film of 2.6 μm in thickness deposited onto a tool steel substrate, the direct determination of the hardness and elastic modulus of the film leads to values of 35.5 ± 2 GPa and 490 ± 50 GPa, respectively.

1. Introduction

The determination of the mechanical properties of thin films by nanoindentation often requires the application of models for separating the contribution of the substrate from the indentation data. For hardness measurement, the models must be applied as soon as the indenter displacement is higher than ~10% of the film thickness [1,2]. When considering the elastic modulus determination, the indenter displacement must be less than a limiting value, which depends on the mechanical properties of both of the film and of the substrate. This limiting value is close to ~1% of the film thickness for a hard film deposited onto a soft substrate [3,4] and it can reach ~20% for a soft film deposited onto a hard substrate [5,6].

To avoid the application of such models for which the above mentioned limiting values cannot be defined precisely and whose accuracy depends significantly on the adjustment parameters intrinsic to each model, a direct determination of the mechanical properties of the material will sometimes be preferable. However such a determination requires reliable indentation data at very low indenter displacements and as the film thickness decreases. This concerns the computation of the contact indentation depth and contact area, both used in the methodology of Oliver and Pharr [7] for determining the elastic modulus and hardness.

In these conditions, the unavoidable presence of a rounded indenter tip due to the bluntness of the indenter must be taken into account to limit the deviation from the usual values of the contact area. Whereas a simple additional term is sufficient for calculating the indenter displacement, the contact area computation requires a much more complex formulation.

To take into account the effect of the indenter tip-rounding on the determination of the projected contact area, Oliver and Pharr [7] proposed a complex phenomenological area function for a Berkovich indenter, which involves several constants necessary for the description

* Corresponding author.
E-mail address: didier.chicot@univ-lille1.fr (D. Chicot).

of the deviation from the perfect Berkovich indenter. However, even if the area description is very precise, the determination of the coefficients involves a complex iteration procedure until convergence is achieved. Moreover, Sawa and Tanaka [8] have pointed out that the resultant area function depends on the initial guess values employed for the iteration.

On the other hand, Gong et al. [9] added that it is very difficult to attribute a clear physical meaning to the descriptive parameters of this area function. However and independently on the scientific debate about the meaning of these parameters, it is important to indicate that this phenomenological area function leads, in our opinion, to the best computation of the contact area. However, one problem which remains to be solved concerning the general use of this formulation is that this area function is only applicable when employing the continuous stiffness measurement (CSM) mode.

Consequently, to avoid this limitation, some authors [10–16] have proposed the use of a simple polynomial of second degree, in which some physical meaning has been attributed to the different parameters involved. These authors have usually employed two parameters: i) one, which describes the angle deviation from the theoretical effective conical angle of 70.32° and ii) a second one, which concerns the tip defect and which can be represented by the effective truncation length or the radius of the rounded indenter tip.

Despite their interest in microindentation, it is widely recognized that such simple polynomial laws cannot be validly applied for indenter displacements less than a depth value close to 200 nm. Unfortunately, this limiting value is not small enough for the mechanical characterization of very thin films, to avoid the influence of the substrate. Within this objective, Franco et al. [17] proposed an area function by introducing two empirical parameters. For Liu et al. [18], the polynomial function is of 4th degree, thus multiplying the adjustment coefficients. These approaches are not totally satisfactory since no clear physical meaning is given to the fitting parameters. In addition, a calibration procedure is always required, thus limiting its use.

To obtain a better description of the contact area function for very low indenter displacements and to give physical meaning to the adjustment parameters, Antunes et al. [19] and Berla et al. [20] proposed two comparable area functions consisting of the addition of two terms (linear and exponential) to calculate the calibrated plastic depth. The linear term mainly represents the highest displacements where the fitting parameter is related to the apical angle deviation. The exponential term defines the imperfection tip where one of its fitting parameters is directly connected to the effective truncation length of the indenter tip and the second one indicates the way in which the linear part of the curve is approached. The relationship proposed by Berla et al. [20] only considers the sphere radius representative of the rounded tip with no addition of any fitting parameters.

To avoid a calibration procedure, in the present work a contact area function has been proposed, which takes into account the truncation length of the indenter tip defect in a similar way to the models of Antunes et al. [19] and Berla et al. [20]. The main advantage of the proposed model, as compared to the other ones, is that it can be applied to microindentation data, where the CSM mode is not available and where the calibration procedure using fused silica is not possible due to the formation of cracks around the indent at typical microindentation loads, *e.g.* loads higher than approximately 0.1 N.

In practice, the proposed contact area function is applicable without any calibration procedure if the truncation length is previously determined by means of high resolution microscopy. When compared to the model of Troyon and Huang [14], which is the most widely used in microindentation, it is observed that the proposed area function allows a better analysis in the range of indenter displacements between 10 and 200 nm. Finally, the correction proposed is applied to the determination of the elastic modulus and hardness of a TiHfCN thin film of 2.6 μm of thickness by nanoindentation.

2. Brief description of the existing contact area functions

The determination of the contact area function is usually performed using fused silica, whose elastic modulus and Poisson's ratio are 72 GPa and 0.17, respectively. By analyzing the unloading part of a load–depth curve obtained by instrumented indentation, Oliver and Pharr [7] proposed the correlation of the contact area, A_C, with the reduced modulus, E_R, by means of the total compliance of the system, C, and the frame compliance of the instrument, C_f, as follows:

$$\sqrt{A_C} = \frac{\sqrt{\pi}}{2}\frac{1}{\beta}\frac{1}{\left(C - C_f\right)}\frac{1}{E_R} \tag{1}$$

where β is a correction factor, whose value differs according to the authors [21]. For example, according to King's finite element calculations [22], for the Berkovich indenter, $\beta = 1.034$. On the other hand, $C = \mathrm{d}h/\mathrm{d}P$ and represents the total compliance of the system, i.e. the inverse of the slope of the load (P) versus penetration depth (h) curve at the beginning of the unloading. C_f is supposed to have a constant value in nanoindentation.

E_R is expressed as a function of E_m, E_i, ν_m and ν_i, which in turn represent the elastic modulus and Poisson's ratio of the material and of the indenter, respectively. For a diamond indenter, $E_i = 1140$ GPa and $\nu_i = 0.07$:

$$\frac{1}{E_R} = \frac{1-\nu_m^2}{E_m} + \frac{1-\nu_i^2}{E_i} \tag{2}$$

For fused silica, the reduced modulus is then equal to 69.6 GPa.

For a perfect Berkovich indenter, the projected contact area, A_C, included in Eq. (1) is a function of the contact depth [23], h_c, and it is expressed as follows:

$$A_C = \pi \cdot \tan^2\psi \cdot h_c^2 = 24.56 \cdot h_c^2 \tag{3}$$

where $\psi = 70.32°$ and represents the effective semi-angle of the conical indenter equivalent to the Berkovich one.

To take into account the bluntness of the indenter, Oliver and Pharr [7] proposed the following area function applicable to a Berkovich indenter:

$$A_C = 24.56 h_c^2 + C_1 h_c^1 + C_2 h_c^{1/2} + C_3 h_c^{1/4} + \ldots + C_8 h_c^{1/128} \tag{4}$$

where C_1 through C_8 are constants. The leading term describes a perfect pyramidal indenter; the others describe deviations from the conical geometry due to blunting at the tip.

To reduce the number of constants and to give physical meaning to the fitting parameters, a variety of second degree polynomial describing the contact area function versus the contact depth has been proposed. For example, Hermann et al. [10,11] proposed the plot of the square root of the theoretical contact area as a linear function of the contact depth as follows:

$$\sqrt{A_C} = a h_c + b \tag{5}$$

where a and b are fitting parameters.

For Thurn and Cook [12], it is more convenient to use the following but similar relation:

$$\sqrt{A_C} = \frac{h_c}{C_1} + \frac{C_1}{C_2} \text{ with } C_1 = \frac{1}{\sqrt{\pi}\tan\psi} \text{ and } C_2 = \frac{1}{2\pi R} \tag{6}$$

where R is the effective tip radius, thus giving physical meaning to the coefficients a and b of the relationship proposed by Hermann et al. [10,11] in Eq. (5).

Similarly, Troyon and Huang [14] introduced the effective truncation length of the indenter tip, h_b, and the apical angle as follows:

$$\sqrt{A_C} = \alpha \cdot \sqrt{\pi} \tan\psi \cdot (h_c + h_b) \quad (7)$$

Nevertheless, this is consistent enough for indenter displacements higher than about 200 nm, but the constant term prevents the contact area from taking the value of zero, as the contact depth approaches zero; it becomes significant relative to A_C only at extremely shallow indentation penetrations where the indenter tip can be considered as a sphere.

For obtaining a null value for the contact area when the contact depth equals zero, Franco et al. [17] suggested the multiplication of the theoretical contact area by a power law as follows:

$$\sqrt{A_C} = \sqrt{\pi} \cdot \tan\psi \cdot h_c \left(1 + k h_c^n\right)^{1/2} \quad (8)$$

where k and n are also fitting parameters.

Due to the presence of the parameters k and n in the above relationship, the application of the model of Bei et al. [13] is preferred. These authors suggested the use of a polynomial of second degree, where the constant term is not considered:

$$A_C = \alpha_1 h_c^2 + \alpha_2 h_c \quad (9)$$

In the above equation α_1 must be equal to 24.56 for a perfect Berkovich indenter and the second term α_2 describes a spherical indenter in the limit, when $h_c << R$. α_2 is equal to $2\pi R$.

Another model was proposed by Antunes et al. [19]. It consists of the addition of two terms (linear and exponential) as follows:

$$\sqrt{A_C} = (\sqrt{\pi}\tan\psi) \cdot \left[k_1 h_c + k_2\left(1 - \exp\left[-h_c \frac{k_3}{k_2}\right]\right)\right] \quad (10)$$

where the constant k_1 indicates the deviation of the tip angle (a value different from 1 indicates an incorrect apical angle), whereas k_2 defines the size of the imperfection at the tip. According to the authors, k_3 indicates the way in which the linear part of the curve is approached.

Berla et al. [20] proposed a similar relationship for the contact area function, where one of the differences is the exponent of the contact depth into the exponential term, being 0.5 for Berla et al. [20] instead of 1 for Antunes et al. [19]:

$$\sqrt{A_C} = (\sqrt{\pi}\tan\psi) \quad (11)$$
$$x\left[h_c + \frac{3\sqrt{3}}{2\pi}\frac{R}{\tan\psi}\left(1 - \exp\left[-\frac{2\pi\tan\psi}{3}\sqrt{\frac{2h_c}{3R}}\right]\right)\right]$$

Thus, only one identified parameter, i.e. R corresponding to the radius of the sphere representative of the rounded tip is involved.

3. Experimental techniques

The TiHfCN film was deposited on a high speed steel substrate (M2), in a HEF TSD400-CD magnetron sputtering unit, using a TiHfCN target brazed on a copper plate. Prior to the deposition, the substrates were polished to a mirror-like finish with 1 μm diamond suspension (Ra ~ 0.05 μm) and then ultrasonically cleaned in ethanol for 10 min. The first step of the deposition process consisted in evacuating the sputtering chamber, with a turbo molecular pump, during a 2 h plateau at about 160 °C to facilitate the desorption of impurities. Then, both substrate and target surfaces were sputter etched in argon plasma with a flow rate of 100 sccm and a bias of −500 V for 30 min.

Finally, the film was deposited by applying the following parameters: bias voltage equal to −150 V and cathode power of 350 W. The deposition time was adjusted to achieve a thickness between 2 and 3 μm. Fig. 1a presents a cross section of the film obtained after polishing,

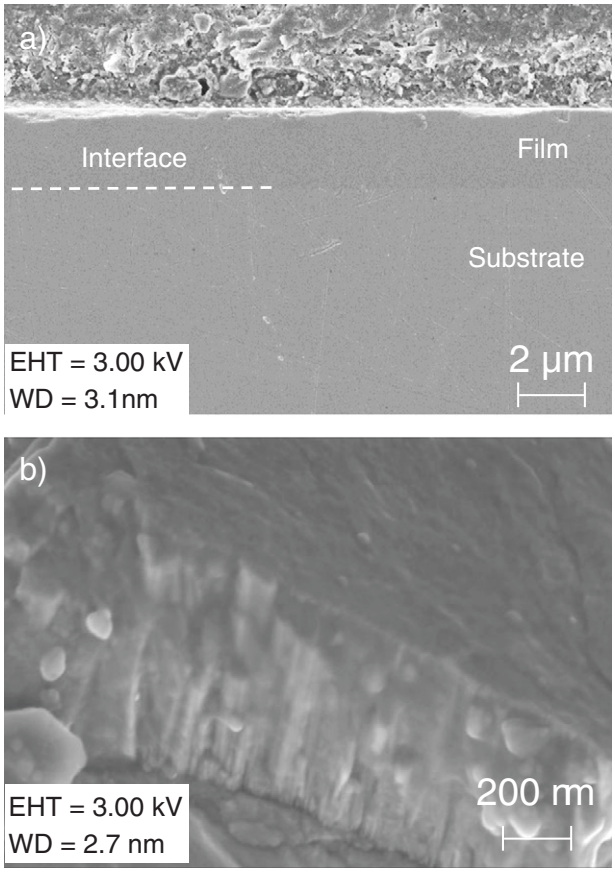

Fig. 1. Cross-section of TiHfCN film (a) after polishing and (b) after fractured in liquid nitrogen.

where it can be observed that the film thickness is of ~2.6 μm. Fig. 1b presents a part of the cross section, which has been fractured in liquid nitrogen to show the typical columnar structure of such physical vapor deposition (PVD) films.

Nanoindentation experiments have been performed employing a Nano Indenter XP™ (MTS Nano Instruments) with a Berkovich indenter. Not less than 30 indentation tests have been conducted randomly at the surface of the coated system by applying the same indentation testing conditions. Considering the main parameters used, the maximum indentation depth reached by the indenter was fixed at 800 nm and the strain rate was equal to 0.05 s^{-1}. The instrument was operated in the continuous stiffness measurement mode (CSM) allowing the determination of the elastic modulus and hardness at every data point acquired during the indentation experiment. The harmonic displacement was 2 nm and the frequency equals to 45 Hz.

To analyze the tip defect of the Berkovich indenter used in nanoindentation, a field emission scanning electronic microscope from HITACHI, type S-4300 SE/N, was employed. The instrument allows the use of an acceleration voltage between 0.5 and 30 kV, which can lead to a resolution of 1.5 nm at an enlargement of 500,000×, at a pressure of 10^{-6} Pa.

4. Experimental results and discussion

4.1. Contact area function analysis using fused silica

In practice, when studying the contact area of Oliver and Pharr, the number of constants of Eq. (4) has been limited to 4. By using the Analyst software from Agilent technologies, the following values have been obtained: $C_1 = 1020$ nm, $C_2 = 2180$ $nm^{3/2}$, $C_3 = -19{,}290$ $nm^{7/4}$

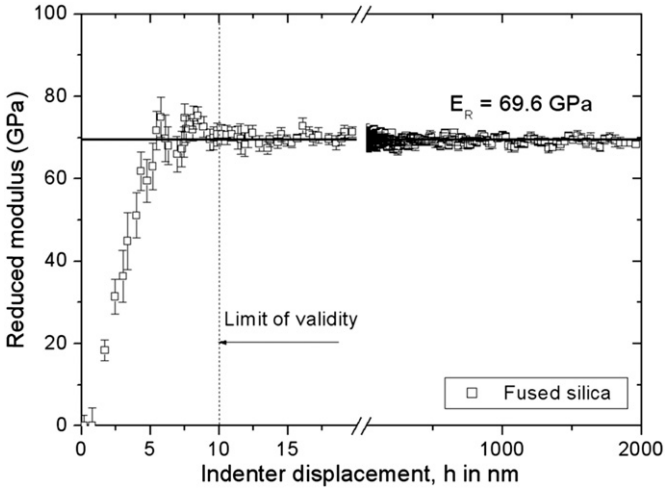

Fig. 2. Reduced modulus of fused silica calculated with the contact area function of the Oliver and Pharr method, as a function of the indenter displacement.

and $C_4 = 16{,}680\ \mathrm{nm}^{15/8}$. Fig. 2 represents the reduced modulus of fused silica as a function of the indenter displacement, where the reduced modulus is calculated with Eq. (1) taking into account the contact area function of Eq. (4) proposed by Oliver and Pharr [7] and the above fitting parameters. It can be observed on Fig. 2 that as soon as the indenter penetration reaches a value between approximately 5 and 10 nm the reduced modulus attains a constant value.

On the other hand, Eqs. (5) to (7) are very similar and allow the plot of the square root of the contact area as a linear function of the contact depth. Fig. 3 shows the use of a linear function for representing the results obtained on the fused silica and the model of Oliver and Pharr for calculating the contact area function. It is clear from Fig. 3 that these contact area functions cannot be applied at very low indenter displacements since when the penetration depth tends to be zero, the contact area exhibits a finite value, which has no physical meaning. For this reason, these authors have probably limited the use of Eqs. (5) to (7) to indenter displacements higher than a value around 100 nm, as indicated in their work.

Thus, the linear regression must be conducted after reaching a critical penetration depth higher than a limiting value, to avoid the contact area deviation between the linear representation and the experimental one clearly visible at the beginning of the indenter penetration. In practice, by considering different critical initial penetration depths chosen between 0 and 200 nm until the last depth value reached by the indenter, different regression coefficients have been obtained, depending on the choice of the initial value. However, it can be observed that the regression coefficients become constant when considering initial limiting displacements higher than 200 nm.

Finally, the regression coefficients indicated in Fig. 3 were obtained from the fit of the indentation data between 200 nm and the maximum contact depth. As a result of this condition of fitting, it is noticeable that the slope is equal to 4.96, which is exactly the theoretical value of the inverse of C_1 in Eq. (6). This result indicates that the value of α in Eq. (7), due to Troyon and Huang [14], is equal to one. Starting from the values indicated in Fig. 3, the radius R of Eq. (6) is found to be equal to 75.4 nm, whereas the effective truncation length of the indenter tip, h_b, of Eq. (7) is equal to 19.3 nm. Note that the geometrical relation between the radius and the tip defect [24] leads to contradictory results between Eqs. (6) and (7) since the radius to tip defect ratio is close to 16.7. As a conclusion, such area functions cannot be used for very low indenter displacements.

The use of the model advanced by Bei et al. [13] (Eq. (9)) with the data obtained from fused silica allows an adequate representation of the contact area versus the contact depth for indenter displacements higher than a value close to 20 nm, as shown in Fig. 4. Note that the radius R is found to be equal to 175 nm, which is very different from the radius deduced from the model of Thurn and Cook [12]. Moreover, the value of 24 in front of h_c^2 indicates that the effective conical angle is equal to 70.10° instead of 70.32°, which is in the range of the tip angle calibration. Note that this value can be influenced by the lower limiting depth used for calculating the fitting parameters. However, it is noticeable that the previously applied models lead to a perfect effective conical angle, contrary to this model.

The model advanced by Berla et al. [20] (Eq. (11)) probably provides the most useful relationship to compute the contact area function without any fitting parameter, but the radius of the indenter tip remains difficult to estimate. Fig. 5 represents jointly the application of Eq. (10), derived from the Antunes et al. model [19] and Eq. (11), but no significant differences are observed even for very low indenter displacements. As a main result, the two models can be, applied independently over all the range of indenter displacements.

In our study, the model of Antunes et al. [19] gives $k_1 = 1$, thus confirming that the tip angle is equal to 70.32°, $k_2 = 18.1$ nm, which is of the same order of magnitude as h_b, i.e. 19.3 nm, deduced from the model of Troyon and Huang [14] and $k_3 = 1.068$, which in our opinion, does not have a clear physical meaning since, for example, $k_3 = 2.034$ in the work of Antunes et al. [19]. For the model of Berla et al.

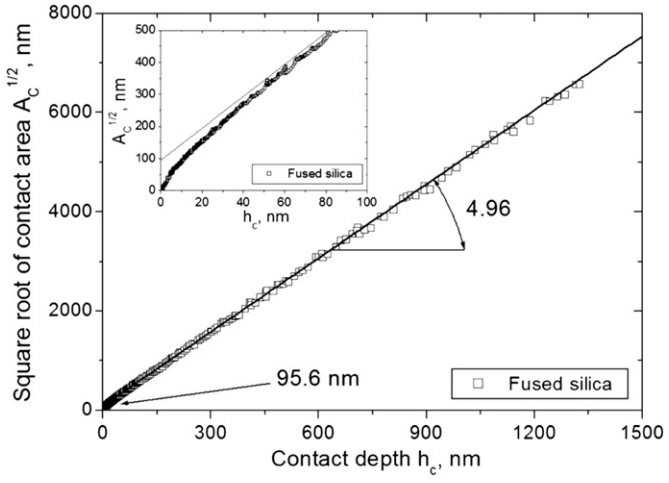

Fig. 3. Theoretical square root of contact area calculated with the model of Oliver and Pharr as a function of the contact depth for fused silica.

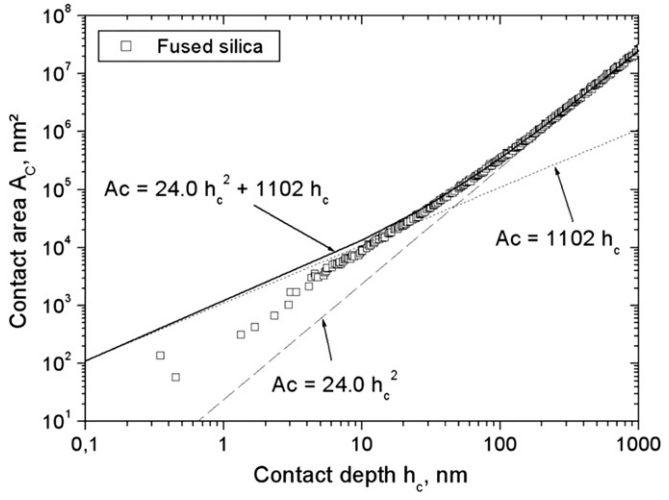

Fig. 4. Contact area calculated with the model of Oliver and Pharr versus contact depth represented by the model of Bei et al. [13].

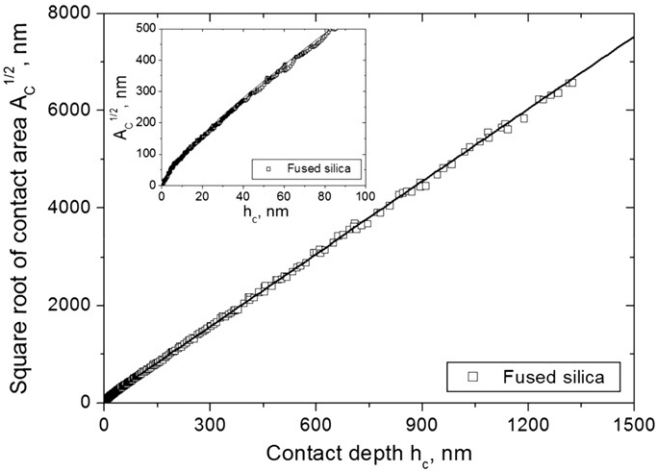

Fig. 5. Square root of contact area calculated with the model of Oliver and Pharr as a function of the contact depth corresponding to application of Eqs. (11) and (12).

[20], the radius $R = 74.0$ nm, which is very close to 75.4 nm obtained by the model of Thurn and Cook [12].

As a main conclusion, the different models can be applied but their choice will depend on the depth range required for the indentation analysis, which in turn depends on the type of sample and characterization features. In any case, it can be observed that most of these models require a calibration procedure for the determination of the fitting parameters and/or the indentation test is conducted under the CSM mode.

In microindentation, where application of the CSM mode is not possible, the model of Troyon and Huang [14] involving only the truncation length without any fitting parameters is usually applied since its domain of validity is reduced to depths higher than a value around 200 nm. To reduce this limiting value to only few nanometers, a model based on the functions developed by Antunes et al. [19] and by Berla et al. [20] is then proposed:

$$\sqrt{A_C} = (\sqrt{\pi}\tan\psi)\cdot\left[h_c + h_b\left(1-\exp\left[-2\frac{h_c}{h_b}\right]\right)^{3/2}\right] \quad (12)$$

where the effective truncation length of the indenter tip, h_b, can be determined by regression analysis or estimated from microscopic observations.

In the present work, Eq. (12) is applied to the study of fused silica for determining the truncation length h_b, which will be afterward compared to its estimation by high resolution scanning electron microscopy. To determine its value, the square root of the contact area is plotted as a function of the contact depth, as illustrated in Fig. 6a. The indentation data are then fitted by Eq. (12), which adequately describes the experimental data in the same manner as the different models described above. It has been found that the value of the truncation length is of approximately 15.2 nm, which is very close to the values obtained by the other models.

It is important to observe that the value of h_b can also be roughly estimated by means of linear regression on large depth data after 200 nm in depth, by neglecting the exponential term and thus avoiding the calibration procedure and the estimation of the tip defect by microscopy. This methodology is analog to the use of the model of Troyon and Huang [14] (Eq. (7)) when it is assumed that $\alpha = 1$.

However, when using the contact area function (Eq. (12)) to calculate the reduced modulus of fused silica, it is shown that the prediction is very accurate for indenter displacements higher than 50 nm, whereas a deviation between 10 and 50 nm of penetration depth (Fig. 6b) can be observed. Note that this deviation is quite acceptable since the variation is located between ±5% of the mean value of the

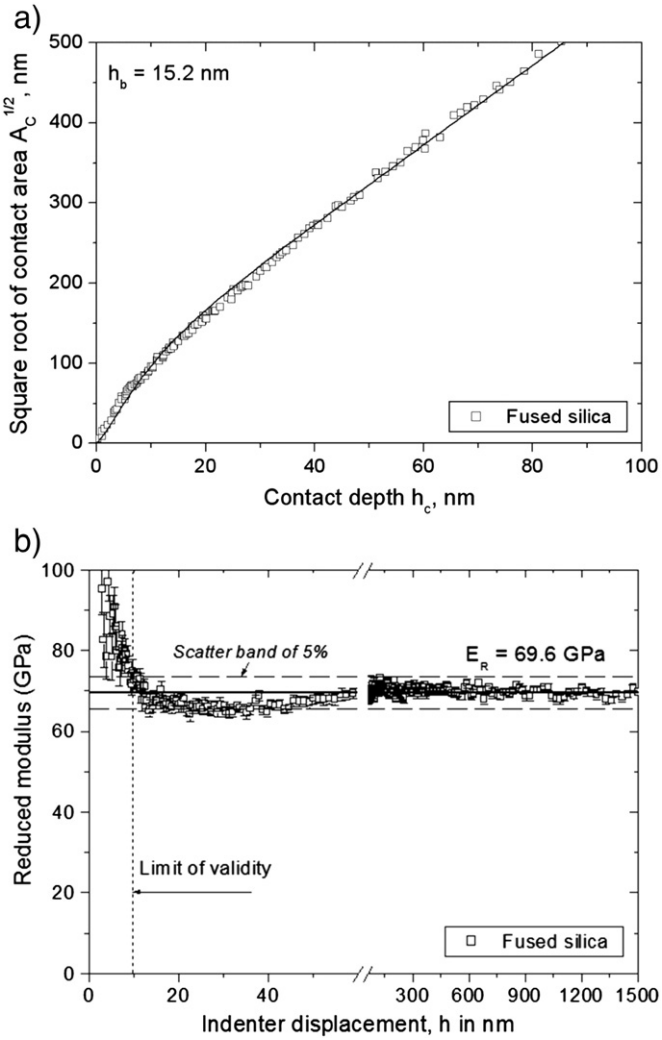

Fig. 6. (a) Square root of contact area function of the contact depth, Eq. (13). (b) Reduced modulus versus indenter displacement corresponding to the application of Eq. (13) to the indentation data obtained on the fused silica.

reduced modulus, which is a standard deviation usually accepted for the elastic modulus.

Moreover, it is important to note that the application of the models of Antunes et al. [19] and Berla et al. [20] show the same typical variation for the lowest indenter displacements, contrary to the model of Oliver and Pharr [7], which is very precise until depths close to 10 nm, as shown on Fig. 2. Nevertheless, the advantage of such a model as compared to the method of Oliver and Pharr [7] is that the contact area function can be estimated by the observation of the indenter tip by SEM. Fig. 7 shows a photograph of the indenter-tip under high magnification and high resolution. In this case, the truncation length can be estimated between 15 and 20 nm in accordance to the values found by fit using different contact area functions.

In any case, the proposed model could replace the model of Oliver and Pharr for studying very low indenter displacements, typically lower than 20 nm. For this reason, the application of this model is suggested only when the CSM mode is not available on the indentation equipment.

4.2. Hardness determination of TiHfCN thin film

Now, considering the contact area function of Eq. (12), the contact hardness directly measured on the TiHfCN thin film of 2.6 μm in thickness can be plotted as a function of the indenter displacement, as

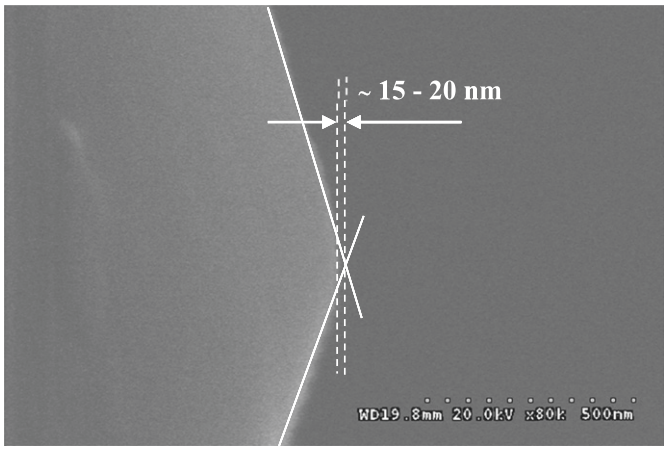

Fig. 7. Evaluation of the size of the tip defect of the Berkovich indenter by mean of emission field SEM analysis at very high magnification using secondary electron beam, 20 kV of acceleration voltage, magnification of ×80K and 51 μA of current.

shown in Fig. 8a. This figure clearly indicates that the hardness of the film is constant and equals to 35.5 ± 3 GPa between 90 and 260 nm. Note that when applying the model of Troyon and Huang [14] (Eq. (7)), a hardness variation is observed in this same range of penetration depths and the hardness tends to decrease when the indenter displacement increases as shown in Fig. 8b. The model of Oliver and Pharr has also been applied on the indentation data determined for the TiHfCN thin film and the obtained result is very similar to the result presented in Fig. 8a, which confirms the good fitting of the contact area by Eq. (12).

However, we can observe that the change in hardness in Fig. 8a appears when the displacement of the indenter is close to 260 nm, which corresponds to 10% of the film thickness accordingly to the general rule given by [1,2]. For the lowest indenter displacements, a fast decrease in hardness is observed for depths lower than 90 nm, a value which is very high as compared to the 10 nm obtained with the calibration sample for the elastic modulus variation. In order to understand the origin of such a difference, the hardness variation obtained under the same condition of calibration performed on the fused silica was plotted by using the same contact area function.

Fig. 9 represents the hardness variation of fused silica calculated with Eq. (12). It is very interesting to note that the same limiting value of 90 nm is observed on the calibration sample as well as on the tested material, whereas this value is equal to 10 nm when considering the reduced modulus (Fig. 6a). When the phenomenological contact area function proposed by Oliver and Pharr [7] is applied, the same trend is observed and the same value is obtained for this limiting depth. For this reason, this limit cannot be related to the inconsistency of the contact area function. Indeed when calibrating the contact area function of Oliver and Pharr [7] by fixing the hardness equal to 9.6 GPa (value usually admitted for the fused silica and validated on Fig. 9 for the highest displacements), the reduced modulus is found to vary to a large extent over 90 nm, whereas the hardness number is constant up to 10 nm in-depth. Finally, the calibration procedure was applied to the phenomenological area function of Oliver and Pharr [7] by fixing the elastic modulus, which is the methodology generally employed in indentation. Afterward, the results obtained were compared with the model proposed, for which no calibration procedure is required. In this case, both the hardness and reduced modulus deduced from the two methodologies converge toward the same values.

As a conclusion, we suggest studying the hardness variation over the displacement range in agreement with the hardness variation obtained on the fused silica sample, i.e. for indenter displacements higher than 90 nm instead of 10 nm, which is the value found when calibrating with the reduced modulus. Finally, Fig. 8a shows that the hardness of the film is constant between 90 and 260 nm thus indicating that the TiHfCN film is not sensitive to the indentation size effect representative of the hardness–indent size variation. So, it is possible to conclude that the hardness of the TiHfCN thin film is effectively equal to 35.5 ± 2 GPa.

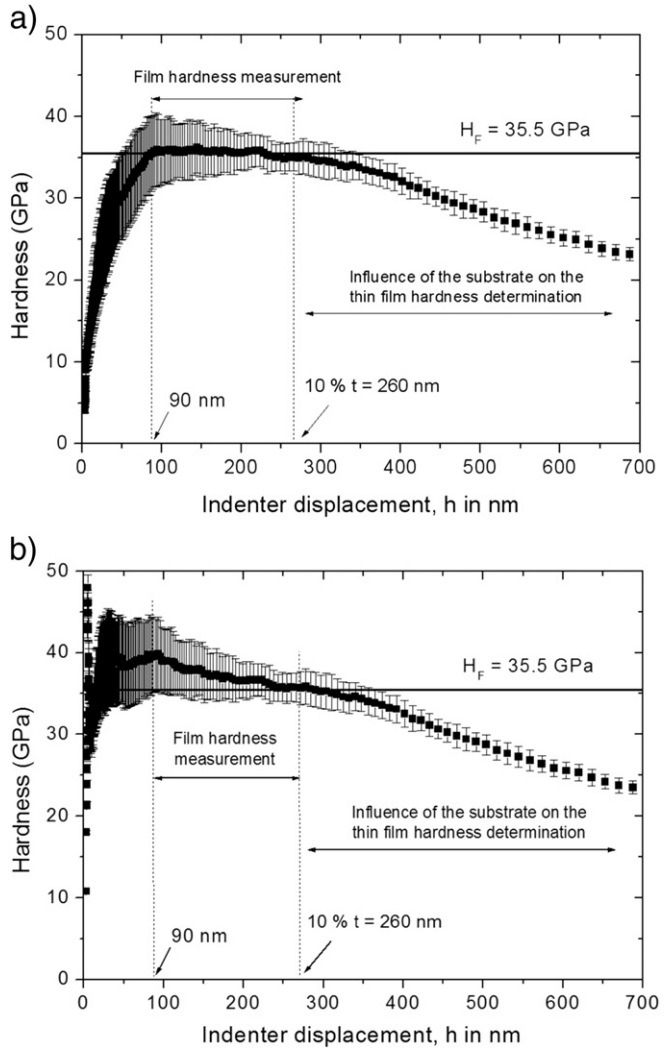

Fig. 8. Hardness determination of the TiHfCN thin film using (a) contact area function in Eq. (13) and (b) contact area function of Eq. (8).

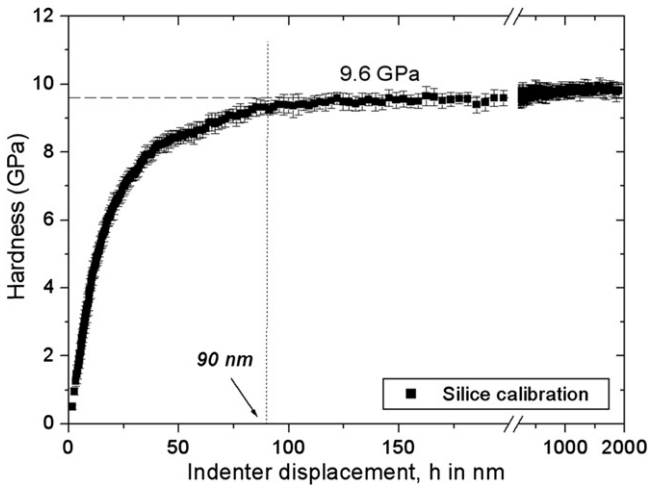

Fig. 9. Contact hardness variation obtained on the calibration sample, i.e. fused silica, using the contact area function in Eq. (13).

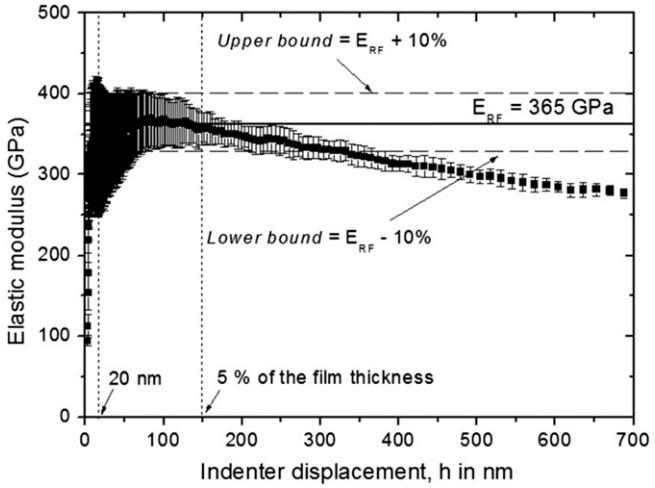

Fig. 10. Elastic modulus variation obtained on the TiHfCN thin film using the contact area function in Eq. (13).

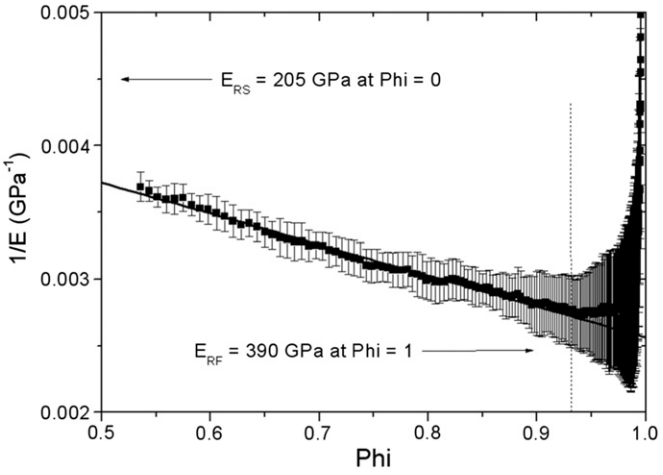

Fig. 11. Model of Antunes et al. [29] representing the reciprocal reduced modulus versus the weight function of Gao [28] applied to the nanoindentation data obtained on the TiHfCN thin film.

Concerning the determination of the elastic modulus of the TiHfCN film, Fig. 10 represents its variation as a function of the indenter displacement, where the reduced modulus is computed taking into account the contact area calculation of Eq. (12). It is noticeable in this figure that the reduced elastic modulus tends to become constant for indenter displacements less than a value close to 150 nm corresponding to 5% of the film thickness of 2.6 μm. Between 20 nm and 150 nm, the reduced modulus is equal to 365 GPa with a variation in the range of ±10% around the mean value. This scatter band is indicated by the upper and lower bounds in Fig. 10. For indenter displacements higher than 150 nm, the reduced elastic modulus decreases toward the value corresponding to the reduced modulus of the substrate. As a conclusion, the elastic modulus of the TiHfCN film is equal to ~490 GPa when considering a value of 0.3 for the Poisson's ratio, when no other value is given for the tested material. Moreover, we can note that the domain of validity for analyzing the elastic modulus variation starts from 20 nm according to the limit obtained with the analysis of fused silica, contrary to the hardness variation which is limited from 90 nm.

Moreover, it is interesting to compare the direct measurement with the results obtained from classical methodologies used when no direct determination of the elastic modulus is possible. Indeed, in these conditions, the application of a model is required. In a previous work [25], different models have been tested on the same thin film. Among the tested models [26–29], that of Antunes et al. [29] led to the best prediction. This model proposes the representation of the composite modulus as a combination of those of the substrate and of the film in relation to the contact indentation depth, h, and the film thickness, t, by means of the weight parameter Φ earlier proposed by Gao et al. [28], as follows:

$$\frac{|1/E_{RC}-1/E_{RS}|}{|1/E_{RF}-1/E_{RS}|}=\Phi=\frac{2}{\pi}\arctan\xi+\frac{1}{2\pi(1-\upsilon)}\left[(1-2\upsilon)\xi\ln\left(\frac{1+\xi^2}{\xi^2}\right)-\frac{\xi}{1+\xi^2}\right] \quad (13)$$

where, for a Berkovich indenter, ξ equals to $(t/[h\cdot\tan\psi])$ and ψ is the effective semi-angle of an equivalent conical indenter (70.32°).

Fig. 11 represents the reciprocal of the reduced modulus as a function of the weight parameter and, as expected according to Eq. (13), the variation can be adequately represented by a straight line over a large range of phi values. When such a line is extrapolated to a value of $\Phi = 1$, the reduced modulus of the film can be obtained. In this case, it takes a value of 390 GPa, which leads to an elastic modulus of 540 GPa for the TiHfCN film. This result differs approximately in 10% from a value of 490 GPa found by means of the direct determination of the reduced modulus of the film.

It is important to note that the difference between the predicted value by means of Gao's function and the actual value can diverge to a large extent depending on the two elastic properties of the film and the substrate and of the film thickness. To estimate this deviation between the two extreme elastic modulus values, a schematic representation of the elastic modulus variation as a function of phi is presented in Fig. 12. The deviation is indicated by ΔE and is equal to $(E_{fA} - E_{fP})$, where E_{fA} represents the actual elastic modulus of the film and E_{fP} its predicted value by the model. The magnitude of this difference is related to the total distance over which the substrate does not interfere with the elastic modulus measurement, that is to say when the indenter displacement is lower than a given fraction of the film thickness defining h_{lim}, and to the ratio between the substrate and the film elastic moduli (E_f/E_s). As an example, when the film thickness has a high value and when the elastic moduli of film and substrate are very different, the predicted value can be very different from the actual elastic modulus of the film.

To conclude, it is noticeable that similar values for the elastic modulus of this film have been given in the literature. Indeed, the TiHfCN target supplier has indicated an elastic modulus of 425 GPa. Moreover, Yang

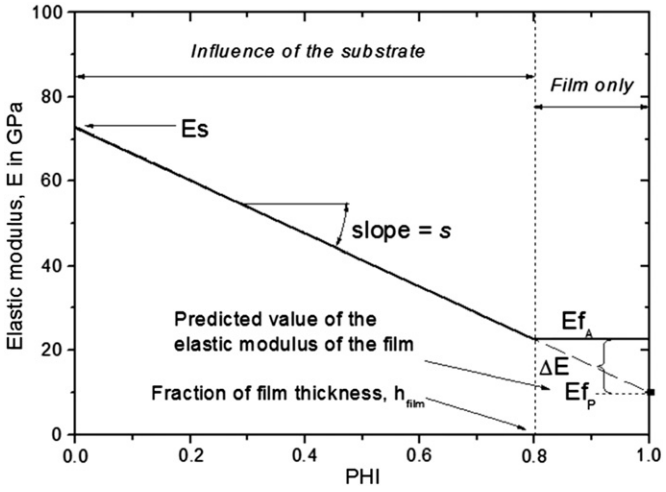

Fig. 12. Schematic representation of the composite elastic modulus versus a function depending on the indenter displacement, h, the film thickness, t, and a fitting parameter, α_t.

et al. [30] have measured Young's moduli of 450 GPa, 370 GPa and 410–450 GPa for bulk $Ti(C_xN_{1-x})$, $Ti(C_xN_{1-x})_{0.81}$ and $Hf(C_xN_{1-x})$, respectively, depending on the [C]/([C] + [N]) ratio. Considering other results obtained on different films, values between 150 and 250 GPa have been reported for TiCN deposited by magnetron sputtering [31], whereas Lugscheider et al. [32] have reported values between 380 and 600 GPa for TiHfCrN supperlattice thin films obtained by arc-PVD.

5. Conclusions

The determination of consistent values of the mechanical properties of materials by means of indentation techniques requires necessarily the consideration of the indenter tip defect influence. Therefore, to compute the contact area, an alternative approach for a Berkovich indenter is proposed, where only the truncation length of the indenter-tip defect is incorporated into the model. It has been determined that the contact area calibration and the mechanical characterization of a thin film by applying the model proposed are nearly as good as those obtained by means of the Oliver and Pharr's phenomenological polynomial function and better than those determined with other existing models, using only the same indenter tip defect parameter.

In addition, the proposed contact area function exhibits additional features: i) the function can be applied when the truncation length is previously estimated by high resolution microscopy, ii) the function can be easily calibrated by conducting a linear fit to large-depth data by neglecting the deviation observed at very low indenter displacements lower than 200 nm and iii) the function is expected to be robust over a large range of indenter displacements. Considering all these aspects, it can be concluded that the model proposed can effectively be used as the contact area function for indenter calibrations, although the quality of the calibrations at the smallest depths may be questionable since a deviation of 5% has been observed when determining the elastic modulus for distances less than 50 nm. Finally, although the model proposed specifically describes three-sided pyramidal indenters, it could be extended for describing conical indenters by making an estimation of the indenter-tip defect. When this model is applied to the mechanical characterization of a TiHfCN film, values of 35.5 $\pm$ 2 GPa and 490 $\pm$ 50 GPa are determined for the hardness and elastic modulus of the film, respectively.

Acknowledgments

Professor Puchi-Cabrera gratefully acknowledges the financial support of the Conseil Régional Nord-Pas de Calais, France, through the International Chair program 2011.

References

[1] H. Bückle, The Science of Hardness Testing and Its Research Applications, in: J.W. Westbrook, H. Conrad (Eds.), American Society for Metals, OH, 1973, p. 453.
[2] Y. Sun, T. Bell, S. Zheng, Thin Solid Films 258 (1995) 198.
[3] T. Chudoba, N. Schwarzer, F. Richter, Surf. Coat. Technol. 154 (2002) 140.
[4] F. Cleymand, O. Ferry, R. Kouitat, A. Billard, J. von Stebut, Surf. Coat. Technol. 200 (2005) 890.
[5] T. Ohmura, S. Matsuoka, K. Tanaka, T. Yoshida, Thin Solid Films 385 (2001) 198.
[6] Z.H. Xu, D. Rowcliffe, Thin Solid Films 447–448 (2004) 399.
[7] W.C. Oliver, G.M. Pharr, J. Mater. Res. 7 (1992) 1564.
[8] T. Sawa, K. Tanaka, J. Mater. Res. 16 (2001) 3084.
[9] J. Gong, H. Miao, Z. Peng, Mater. Lett. 58 (2004) 1349.
[10] K. Herrmann, N.M. Jennette, W. Wegener, J. Meneve, K. Hasche, R. Seemann, Thin Solid Films 377–378 (2000) 394.
[11] K. Herrmann, K. Hasche, F. Pohlenz, R. Seemann, Measurement 29 (2001) 201.
[12] J. Thurn, R.F. Cook, J. Mater. Res. 17 (2002) 1143.
[13] H. Bei, E.P. George, J.L. Hay, G.M. Pharr, Phys. Rev. Lett. 95 (2005) 045501 (4 pp.).
[14] M. Troyon, L. Huang, Surf. Coat. Technol. 201 (2006) 1613.
[15] H.-J. Weiss, Phys. Status Solidi 99 (1987) 491.
[16] C.H. Ullner, L. Höhne, Phys. Status Solidi 129 (1992) 167.
[17] A.R. Franco Jr., G. Pintaude, A. Sinatora, C.E. Pinedo, A.P. Tschiptschin, Mater. Res. 7 (2004) 483.
[18] S. Liu, Y. Gu, H. Huang, Mater. Sci. Eng. A 528 (2011) 7948.
[19] J.M. Antunes, A. Cavaleiro, L.F. Menezes, M.I. Simoes, J.V. Fernandes, Surf. Coat. Technol. 149 (2002) 27.
[20] L.A. Berla, A.M. Allen, S.M. Han, W.D. Nix, J. Mater. Res. 25 (2010) 735.
[21] D. Chicot, F. Roudet, A. Zaoui, G. Louis, V. Lepingle, Mater. Chem. Phys. 119 (2010) 75.
[22] R.B. King, Int. J. Solids Struct. 23 (1987) 1657.
[23] A.C. Fischer-Cripps, Surf. Coat. Technol. 200 (2006) 4153.
[24] D. Chicot, Mater. Sci. Eng. A 499 (2009) 454.
[25] D. Chicot, E.S. Puchi-Cabrera, R. Aumaitre, G. Bouscarrat, C. Dublanche-Tixier, F. Roudet, M.H. Staia, Thin Solid Films 522 (2012) 304.
[26] M.F. Doerner, W.D. Nix, J. Mater. Res. 1 (1986) 601.
[27] J. Mencik, D. Munz, E. Quandt, E.R. Weppelmann, M.V. Swain, J. Mater. Res. 12 (1997) 2475.
[28] H. Gao, C.H. Chiu, J. Lee, Int. J. Solids Struct. 29 (1992) 2471.
[29] J.M. Antunes, J.V. Fernandes, N.A. Sakharova, M.C. Oliveira, L.F. Menezes, Int. J. Solids Struct. 44 (2007) 8313.
[30] Q. Yang, W. Lengauer, T. Koch, M. Scheerer, I. Smid, J. Alloys Compd. 309 (2000) L5.
[31] R. Chen, J.P. Tu, D.G. Liu, Y.J. Mai, C.D. Gu, Surf. Coat. Technol. 205 (2011) 5228.
[32] E. Lugscheider, K. Bobzin, C. Pinero, F. Klocke, T. Massmann, Surf. Coat. Technol. 177 (178) (2004) 616.